CO_2 Geologic Storage:
Coupled Hydro-Chemo-Thermo-Mechanical Phenomena
- From Pore-scale Processes to Macroscale Implications -

Final Scientific/Technical Report

2010 - 2013

Principal Investigator

J. Carlos Santamarina

November 2013

DOE Award Number: DE-FE0001826

Georgia Institute of Technology
Atlanta, GA 30332-0355

ABSTRACT

Global energy consumption will increase in the next decades and it is expected to largely rely on fossil fuels. The use of fossil fuels is intimately related to CO_2 emissions and the potential for global warming. Geological CO_2 storage aims to mitigate the global warming problem by sequestering CO_2 underground. Coupled hydro-chemo-mechanical phenomena determine the successful operation and long term stability of CO_2 geological storage.

This research explores coupled phenomena, identifies different zones in the storage reservoir, and investigates their implications in CO_2 geological storage. In particular, the research: Explores spatial patterns in mineral dissolution and precipitation (comprehensive mass balance formulation); experimentally determines the interfacial properties of water, mineral, and CO_2 systems (including CO_2-water-surfactant mixtures to reduce the CO_2-water interfacial tension in view of enhanced sweep efficiency); analyzes the interaction between clay particles and CO_2, and the response of sediment layers to the presence of CO_2 using specially designed experimental setups and complementary analyses; couples advective and diffusive mass transport of species, together with mineral dissolution to explore pore changes during advection of CO_2-dissolved water along a rock fracture; upscales results to a porous medium using pore network simulations; measures CO_2 breakthrough in highly compacted fine-grained sediments, shale and cement specimens; explores sealing strategies; and experimentally measures CO_2-CH_4 replacement in hydrate-bearing sediments during. Analytical, experimental and numerical results obtained in this study can be used to identify optimal CO_2 injection and reservoir-healing strategies to maximize the efficiency of CO_2 injection and to attain long-term storage.

TABLE OF CONTENTS

EXECUTIVE SUMMARY

Global energy consumption will increase in the next decades and it is expected to largely rely on fossil fuels. The use of fossil fuels is intimately related to CO_2 emissions and the potential for global warming. Geological CO_2 storage aims to mitigate the global warming problem by sequestering CO_2 underground. Coupled hydro-chemo-mechanical phenomena determine the successful operation and long term stability of CO_2 geological storage.

The scope of work included general analyses in the governing parameter domain, interfacial properties of water, mineral, CO_2 and/or surfactant system, interaction between clay particles and CO_2, reactive fluid flow as a result of CO_2 dissolution, two-phase flow between immiscible CO_2 and formation fluid, CO_2 breakthrough and sealing strategies, and CH_4-CO_2 hydrate replacement and hydro-mechanical implications.

We explored coupled phenomena, identified different zones in the storage reservoir, and investigated their implications in CO_2 geological storage. In particular, the research: Explored spatial patterns in mineral dissolution and precipitation (comprehensive mass balance formulation); experimentally determined the interfacial properties of water, mineral, and CO_2 systems (including CO_2-water-surfactant mixtures to reduce the CO_2-water interfacial tension in view of enhanced sweep efficiency); analyzed the interaction between clay particles and CO_2, and the response of sediment layers to the presence of CO_2 using specially designed experimental setups and complementary analyses; coupled advective and diffusive mass transport of species, together with mineral dissolution to explore pore changes during advection of CO_2-dissolved water along a rock fracture; upscaled results to a porous medium using pore network simulations; measures CO_2 breakthrough in highly compacted fine-grained sediments, shale and cement specimens; explored sealing strategies; and experimentally measured CO_2-CH_4 replacement in hydrate-bearing sediments during.

Analytical, experimental and numerical results obtained in this study can be used to identify optimal CO_2 injection and reservoir-healing strategies to maximize the efficiency of CO_2 injection and to attain long-term storage. A selection of important observations follows.

- Four different zones are identified in the reservoir around injection wells, staring from far-field, to intermediate zone, and to near-well zone. In leveled sediments, the CO_2 pool thickness may be limited by lateral capillary trapping rather than by the sediment layer thickness. Typical pools will be only a few meters thick in the absence of geometric traps.
- CO_2-water interfacial tension decreases significantly from 72mN/m to ~25mN/m as pressure increases to reservoir pressure-temperature conditions. Contact angle varies with CO_2 pressure in response to changes in CO_2-water interfacial tension.
- Experimental CO_2 injection tests in pore micro-models and parallel network model simulations demonstrate that the sweep efficiency of CO_2 invasion can be effectively enhanced by lowering the capillary factor. In particular, the sweep efficiency can double with the addition of surfactants.
- The complex interplay between chemo-hydro-mechanical processes may lead to positive feedback mechanisms that can either degrade (e.g., platelet collapse →

increase in pore size → further fluid conduction) or self-stabilize (e.g., water dissolution in CO_2 → salt precipitation from brine → porosity reduction) the caprock seal capacity, or alter CO_2 injectivity into the reservoir.

- Damköhler number and pore-size variability affect the relationship between mean tube diameter and flow rate. Changes in Damköhler number result in inherent bias between average and local trends. Both the Damköhler number and pore-size variability should be accounted in field-scale FEM models.
- Hydro-chemical coupling can lead to dissolution localization (pipes or wormholes) and the formation of shear fractures in compression as the result of the positive feedback that involves changes in porosity and reactive transport. Marked force chains are preferentially vertical away from pipes, yet, they are preferentially horizontal within pipes. Horizontal contact forces inside pipes prevent the buckling of granular columns in the stable zones.
- Leaks in most storage sites will be advection-controlled once percolation takes place (in the absence of high conductivity geological features). Diffusive and advective CO_2 leaks through non-fractured caprocks will be minor and will not compromise the storage capacity of CO_2 injection sites.
- Suspensions of sub-micron clay particles can be injected to fill cracks. Sealing treatments cause a marked increase in the shut-off pressure, and a pronounced decrease in leak rates can be attained as the specimen is subjected to successive sealing treatments.
- CH_4-CO_2 replacement within the stability field occurs without loss of stiffness in the granular medium. CO_2-flooded sandy reservoirs can remain mechanically stable during and after CH_4 gas production.

INTRODUCTION - METHODOLOGY

The efficient short-term injection and the safe stable long-term geological storage of carbon dioxide can be engineered for known or anticipated isolated processes. However, the main concerns in geological storage are related to those still unrecognized phenomena that can emerge as a consequence of relatively complex, coupled hydro-chemo-thermo-mechanical processes that take place in the geological formation, including the development of positive feedback mechanisms, possible runaway effects, as well as self-healing systems.

The scope of the work included: general analyses to bound the parameter domain for the efficient injection and safe long-term geological storage of CO_2, pore-scale surface interactions, dissolution effects in the context of carbon sequestration, breakthrough and conditions for self-healing, numerical up-scaling for particle scale phonemona as well as pore scale phenomena, and numerical simulation for coupled hydro-chemo-mechanical processes.

Unique experimental studies were implemented using unprecedented high-pressure chambers that allowed for the observation of pore-scale surface interactions as well as processes in the micro-model and in effective stress controlled cells, including the measurement of breakthrough pressure and/or shut-off pressure during CO_2 invasion, and mutual dissolution between CO_2 and water. Experimental results were analyzed using physical, chemical and mechanical concepts and were complemented with analytical solutions and numerical simulations. Discrete element and tube network models allowed upscaling grain and pore-scale phenomena in reactive fluid transport and immiscible two-phase flow, while finite element simulations were used to investigate reactive fluid transport at pore-scale in a full span of dimensionless parameter domain.

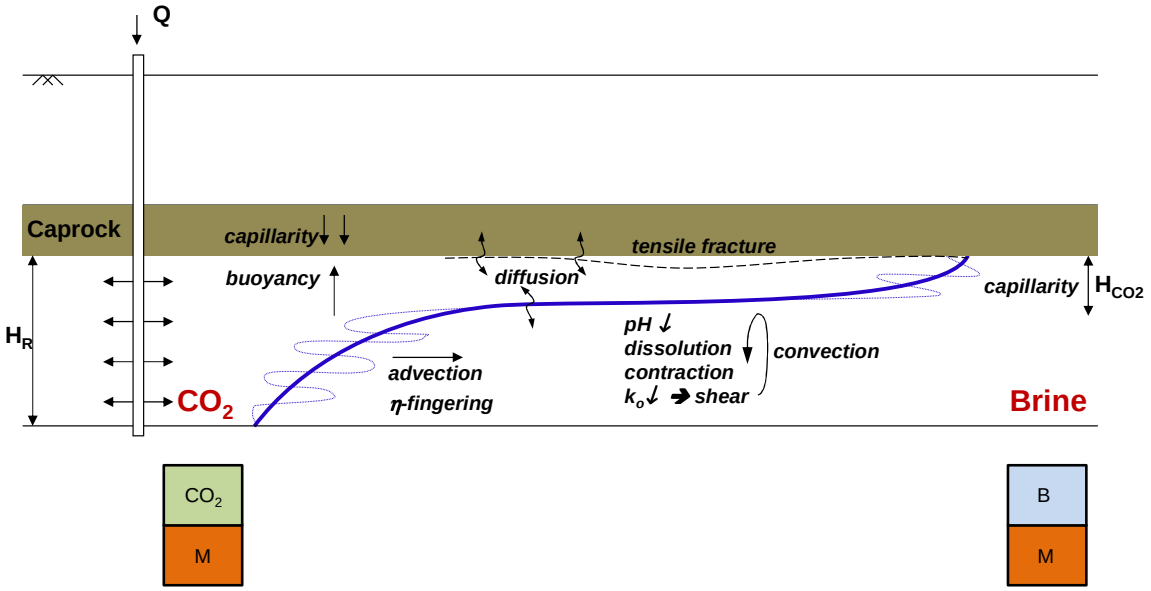

PHYSICAL PROCESSES

General analyses: Hydro-chemo-mechanical analyses and implications

The CO_2 storage reservoir can be analyzed into four different zones around a CO_2 injection well (Figure above). The far-field is not affected by CO_2 injection and brine saturation is S_B=1. Acidified brine dominates the intermediate zone and mineral dissolution prevails over precipitation; loaded with dissolved CO_2 and minerals, denser brine experiences convection and sustains further dissolution in this zone. The ionic strength in brine increases as water is removed by the injected CO_2, and salt precipitation may occur; in fact, brine acidification by CO_2 dissolution and brine dissolution into CO_2 coexist in the transition and there is partial compensation between mineral dissolution and precipitation. The continuous influx of "dry" CO_2 around the injection well, first displaces brine and then dries all the residual brine, resulting in salt precipitation while CO_2 saturation approaches $S_{CO2}\approx 1$.

CO_2 plume thickness. The quasi-static lateral spread of the CO_2 plume in the absence of geometric or stratigraphic features is determined by the balance between the excess buoyant pressure in the CO_2 pool $\Delta\rho \cdot g \cdot H_{CO2}$ and the capillary entry pressure $2T_s/R_{pore}$ required to invade the storage reservoir as predicted by Laplace's equation. Therefore, the CO_2 plume thickness H_{CO2} [m] is a function of the interfacial tension between CO_2 and brine T_s [mN/m], the characteristic pore radius in the storage reservoir R_{pore} [m], and the unit weights of CO_2 and brine, γ_{CO2} and γ_B:

$$H_{CO2} \leq \frac{2T_s}{R_{pore} \cdot (\gamma_B - \gamma_{CO2})}$$

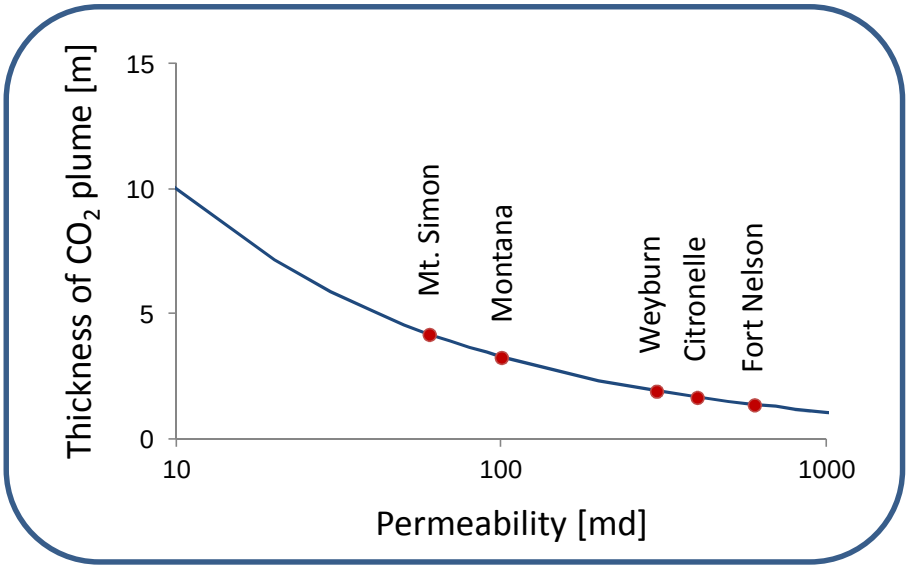

Convection. The Rayleigh number *Ra* compares convective and diffusive transport. For a storage reservoir thickness H_R [m] with permeability k [md], diffusivity D [m^2/s], fluid with viscosity μ [Pa·s], and density difference $\Delta\rho$ [kg/m^3] the Rayleigh number is:

$$Ra = \frac{k \cdot \Delta\rho \cdot g \cdot H_R}{\eta \cdot D}$$

Denser CO_2-dissolved brine triggers instability when $Ra>4\pi^2$. Persistent convective flow may sustain CO_2 dissolution in brine, brine acidification, and ensuing mineral dissolution. The time for convection is $t_{conv}=H_R/v_{conv}$ where the Darcy velocity v_{conv} [m/s]$=k\cdot\Delta\rho\cdot g/\eta$ is a function of the fluid density difference $\Delta\rho$, the hydraulic conductivity k, and the fluid viscosity η:

$$t_{conv} = \frac{\eta \cdot H_R}{k \cdot \Delta\rho \cdot g}$$

For a typical storage reservoir with permeability k=200md, thickness H_R=10m, and density difference $\Delta\rho$=20kg/m^3, the Rayleigh number is $Ra=4.4*10^3>4\pi^2$, convective fingering will take place, and convective fingers will touch the bottom of the reservoir after $t_{conv}\approx$9 years. The mineral flux rate due to convection is in the order of $\Delta V_M\cdot\rho_M/t_{conv}$. While mineral dissolution may be low, short convection times can accumulate substantial mineral flux in through the design time.

Water-CO_2-mineral systems: Interfacial tension, contact angle and diffusion

Previous studies have shown that the interfacial tension and contact angle in CO_2-water-mineral systems change noticeably with fluid pressure. We compile previous results and extend the scope of available data to include saline water, different substrates (quartz, calcite, oil-wet quartz, and PTFE) and a wide pressure range (up-to-20MPa at 298K). Data analysis provides interfacial tension and contact angle as a function of fluid pressure; in addition we recover the diffusion coefficient of water in liquid CO_2 from long-term observations. Results show that CO_2-water interfacial tension decreases significantly as pressure increases in agreement with previous studies. Contact angle varies with CO_2 pressure in all experiments in response to changes in CO_2-water interfacial tension: it increases on non-wetting surfaces such as PTFE and oil-wet quartz; and slightly decreases in water-wet quartz and calcite surfaces. Water solubility and its high diffusivity (from $D=20\times10^{-9}$m^2/s to 200×10^{-9}m^2/s) in liquid CO_2 govern the evolution of inter-particle pendular water. CO_2-derived ionic species interaction with the substrate leads to surface modification if reactions are favorable, e.g. calcite dissolution by carbonic acid and precipitation as water diffuses out of the droplet. Pressure-dependent interfacial tension and contact angle affect injection patterns and breakthrough mechanisms, in other words, the performance of geological formations that act as either reservoirs or seals.

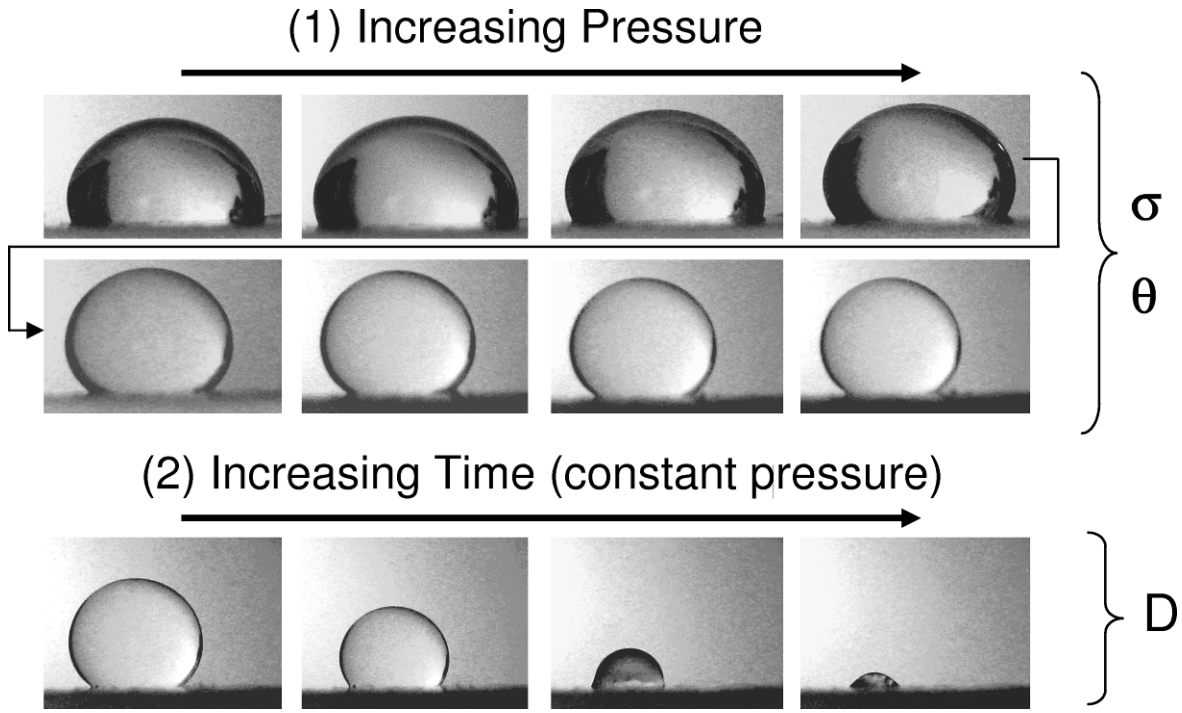

Engineered CO_2 injection

We measured the water-CO_2 interfacial tension and contact angle as a function of pressure, with and without surfactants. The surfactant selected for this study is SURFONIC POA-25R2 (HUNTSMAN), which is a reversed block copolymer composed of hydrophilic polyoxyethylene and CO_2-philic polyoxypropylene. This surfactant is a water soluble, nonionic surface active agent, and has the hydrophilic/lipophilic balance HLB=6.3 (Note: a value HLB=7 denotes even partitioning of surfactants between two phases). High pressure chamber was used for this experimental study: the chamber is first subjected to three cycles of vacuum and CO_2 flushing (99.99% purity) to remove air. At a CO_2 pressure $P \approx 0.1$MPa, water or water mixed with surfactant is injected using a high-pressure syringe to form a droplet that hangs at the tip of a stainless steel needle and/or a sessile droplet that sits on a SiO_2 glass substrate (Note: surfactant concentration wt=0.4%; for reference, the critical micelle concentration is wt=1% at T=28°C-to-32°C; deionized and degased water is used). Thereafter, the chamber is pressurized with CO_2 in steps, from the initial 0.1MPa pressure to 10MPa. A high-resolution camera captures the shape of the droplet through a sapphire window. Recorded images are analyzed using Laplace's equation in parametric form to determine interfacial tension γ_{fl} and contact angle θ.

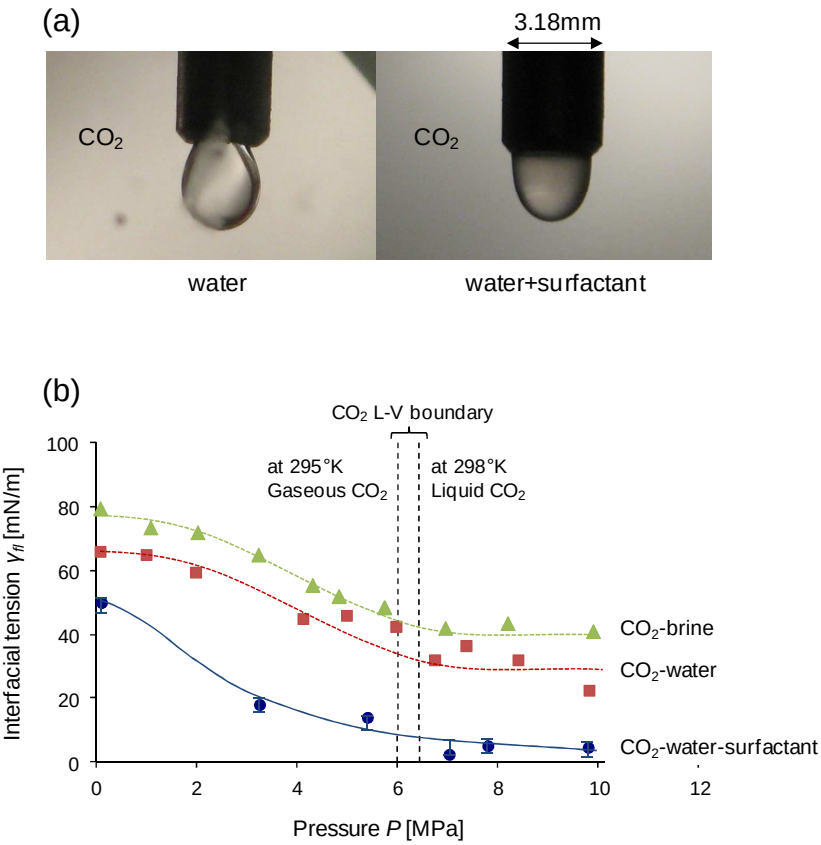

The effect of the surfactant on surface tension is readily seen in the shape of the pendant drop. The addition of surfactant decreases the CO_2-water interfacial tension from ~50mN/m (at 0.1MPa) to a stable value of ~4mN/m when *P*-*T* conditions reach the liquid-gas boundary. The trend parallels the interfacial tension for CO_2-water, with an almost constant shift of 25~35mN/m. Images of sessile droplets sitting on the glass substrate reveal the change in contact angle θ with pressure in the presence of the surfactant. While the contact angle in CO_2-H_2O-SiO_2 remains almost constant as pressure increases, the contact angle increases from θ~20° at *P*=0.1MPa to θ~70° at *P*~10MPa when the surfactant is present. Therefore, the capillary factor in the presence of the surfactant $\gamma_{fl} \cdot cos\theta$ will experience a pronounced decrease as pressure increases.

Clay interaction with liquid and supercritical CO_2

Particle-level forces can be grouped into: (1) mechanical, including skeletal forces due to effective stress, seepage-drag, capillarity, and passive cementation forces; and (2) electrical, including van der Waals attraction, Born repulsion, and electrical forces due to double layer formation, surface hydration and osmotic effects. Because of their physico-chemical nature, electrical forces depend on the pore fluid chemistry.

Study of electrical forces: Sedimentation tests. Sedimentation tests were conducted in a polycarbonate tube (effective height 95mm, ID = 6.35mm and OD = 19.0mm) held between aluminum caps, and sealed with buna-N o-rings. Pressure transducers and thermocouples track pressure-temperature conditions. Time-lapse photography is used to

monitor and record all experiments. The experimental procedure consists of five sequential steps: (1) fill the tube with clay (~0.06g, i.e., the solids volume fraction is less than 0.01), (2) remove adsorbed water on the clay using combined vacuum and heat, (3) fill the tube with the selected fluid (~2.5 ml), (4) shake the cell to thoroughly mix the fluid and clay into a colloidal suspension, and (5) place the tubes vertically, allowing the clay to settle at the bottom of the tubes. This procedure is repeated several times for each clay-fluid combination (2 clays and 5 fluids). We measure the settling rate, sedimentation height, and observe particle agglomeration and flocculation following the test procedure outlined in.

(a) Montmorillonite in distilled water P=0.1MPa and T=298K

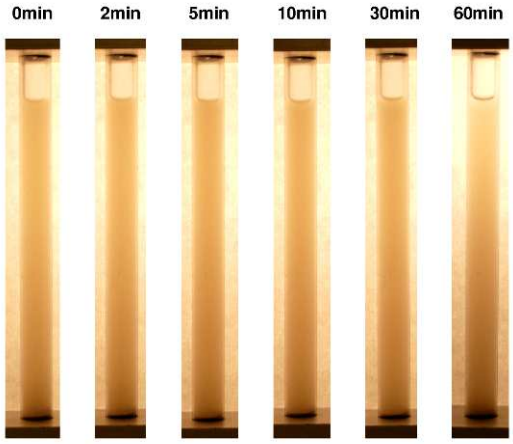

(b) Montmorillonite in scCO$_2$ P=13MPa and T=308K

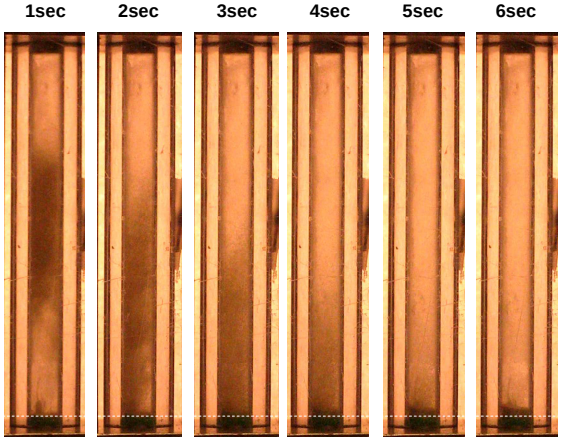

Study of capillary forces: Desiccation tests. Three independent "desiccation experiments" were run by exposing clay-water to a CO_2 atmosphere inside a stainless steel chamber at a temperature T=308-to-313K and pressure P~16MPa. The internal volume of the cylindrical chamber is 210 cm^3. A pressure transducer and a thermocouple are used to monitor pressure and temperature conditions inside the chamber and time-lapse photography is used to observe the evolution of the clay paste through a sapphire window. "Water drying" results from the solubility of water in supercritical CO^2, which reaches ~5×10^{-3} mol of water per mole of CO_2 at 16MPa and 313K, i.e., ~1.5g of water per liter of CO_2.

The test procedure follows: (1) place a 1.5cm^3 of montmorillonite paste (0.1M NaCl solution at an initial water content of 1000%, on a glass slide inside the chamber, (2) remove air and inject dry CO_2 (research grade - Airgas), (3) pressurize to the target pressure-temperature supercritical conditions, and (4) monitor changes in the clay paste at steady temperature and pressure. Periodically, we replaced the wet CO_2 with dry CO_2 under pressure.

a - (+24 h) Water saturated paste	b - (+44.5h) Onset of CO_2 invasion	c - (+60.0h) Extensive localized CO_2 invasion	d - (+73.5 h) CO_2 desiccated clay

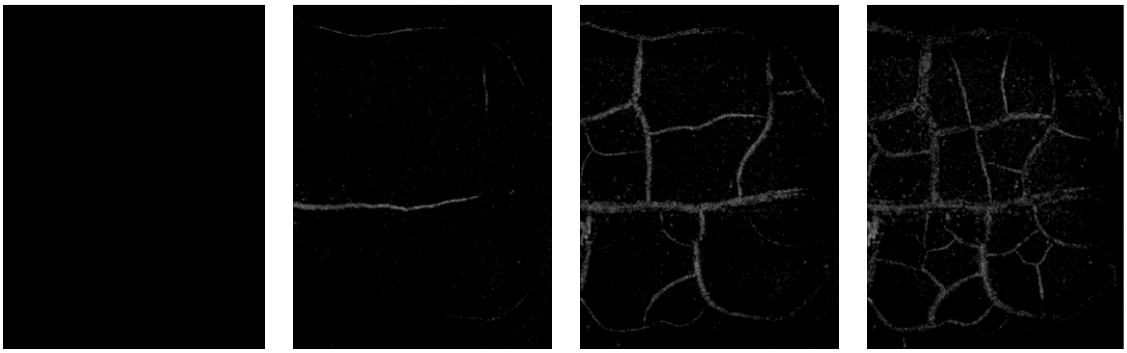

Thresholded images

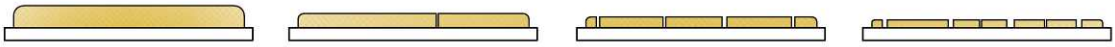

Side view schematics

Reactive fluid transport as a consequence of CO_2 injection

Reactive fluid flow through rock fracture. A numerical simulation study is implemented to explore the coupling between hydro-chemical phenomena during the transport of reactive CO_2-acidified water through a pore in a mineral system. We consider a slice of a rock fracture or a long pore with length l much longer than the aperture d, i.e., $l>>d$, subjected to reactive fluid transport by the forced advection of CO_2-acidified water. The problem is simulated using the moving mesh function in COMSOL to reproduce the fracture enlargement. Flow satisfies the Navier-Stokes' law; species experience both advective and diffusive transport. Mineral dissolution occurs at the interface between the fluid and the joint walls with dissolution rate R_d [mol/m^2/s]. The moving mesh function adjusts the mesh outwards or inwards according to the volume of dissolved mineral $R_d \cdot (v_s/v) \cdot V_m$ [m/s], where (v_s/v) denotes the stoichiometric ratio of dissolved mineral to reactant species and V_m [m^3/mol] is the molar volume of the mineral. We verified the numerical simulation scheme by comparing COMSOL simulation results with a closed-form solution. There is no analytical solution for reactive fluid transport in a two-dimensional pore, so we compare a 1-D analytical solution with 1-D numerical results obtained with COMSOL.

Mineral dissolution couples with advection and diffusion to generate a concentration gradient across and along the pore/joint aperture. Figure below shows a snap-shot of concentrations for all relevant species along a joint in calcite. Low advection velocity allows for diffusion and homogenization across the aperture and for the consumption of most reactant species near the inlet. In contrast, when the advection velocity is high, diffusion fails to homogenize the concentration field across the joint, and mineral dissolution takes place uniformly along the joint length. The longitudinal drop in reactant

species is much lower in the less reactive anorthite for the same advection velocities. For both mineralogies, a higher advection velocity yields higher concentrations of residual reactant species at the outlet due to the lower residence time.

The rock fracture aperture increases as the reactive fluid passes through the fracture plane. Results show that pore enlargement may decrease either exponentially or linearly along the flow path. In all cases, the normalized enlargement $\Delta d/d$ in anorthite is three orders of magnitude lower than that of calcite. For any *Pe* value, a lower *Da* causes the flow channel to experience a more uniform enlargement of the aperture along the joint.

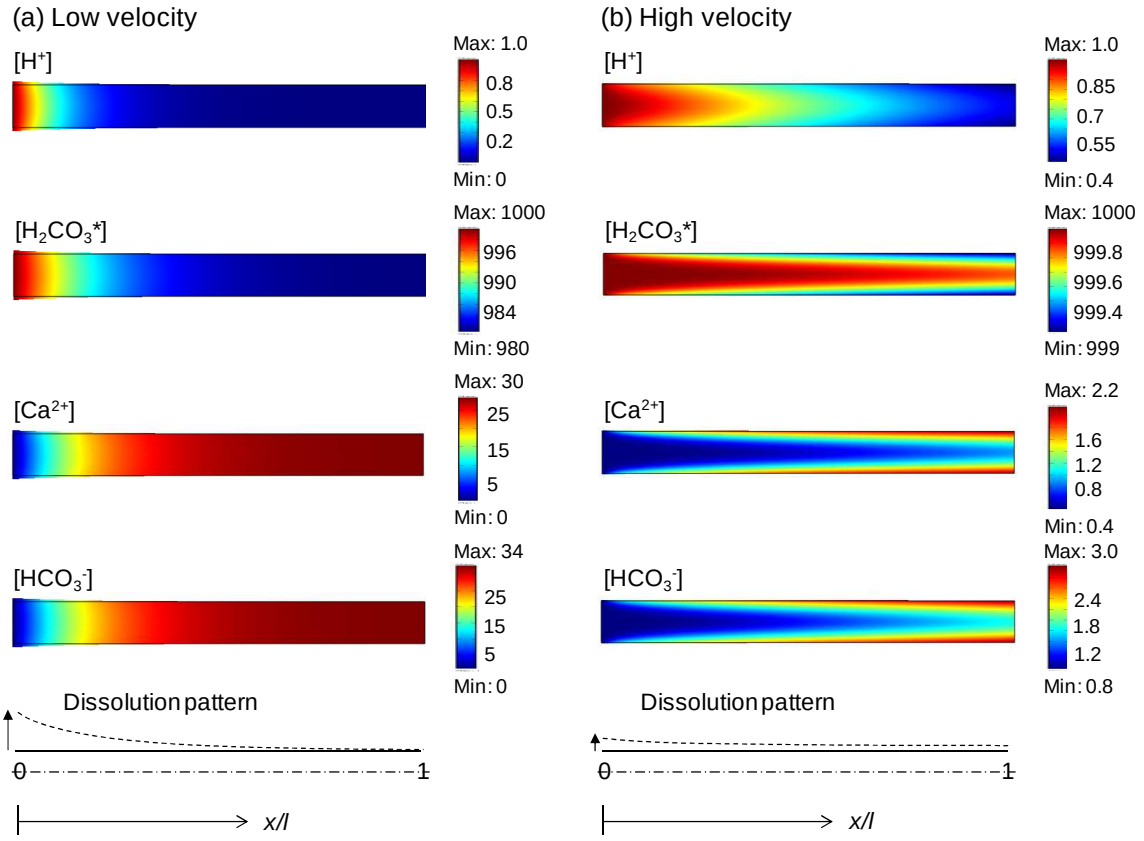

Pore network model study. The 2-D square network consists of tubes that intersect at nodes, where incoming species mix thoroughly. Tube diameters d [m] are log-normally distributed with mean value $\overline{d_0}$ and variance *var*. All tubes have identical length L_{ch} [m]. The limitation in network size NxM is partially overcome by assuming periodic boundary conditions in the transverse direction. Flow is driven by the pressure difference between the inlet P_{in} and the outlet P_{out}.

One cycle in the network simulation corresponds to the time interval Δt, and involves the following steps: (1) estimate the evolution of species concentration at the end of every tube based on species concentrations, velocity, and kinetic rates, (2) compute the enlargement of tube diameter Δd for every tube, (3) update concentration of species at all nodes, and (4) update nodal pressure, velocity and flow rate based on change in tube diameters. We repeat this cycle until the total flushed volume reaches $1000 \cdot V_p$.

We use the numerical algorithm described above to explore dissolution patterns in the context of CO_2 injection projects (for $Da<<1$). The summary of results shows that the reactive flow of water with dissolved CO_2 yields either compact dissolution near the inlet ($Da>10^{-4}$) or several branches of localized flow paths ($Da<10^{-4}$). We also examine the role of pore size variability on the evolution of mean tube diameter and flow rate by running additional simulations with the coefficient of variation COV=1.0 and 1.5. Results show that the normalized flow rate increases faster with higher COV values for a given increase in the normalized mean tube diameter. Hence, the exponent for the Kozeny-Carman equation α increases with pore-size variability. Moreover, the range in the exponent α widens as the coefficient of variation in pore size COV increases: a porous medium with a higher COV is likely to have more localized fluid flow whereby few channels are responsible for most of the flow

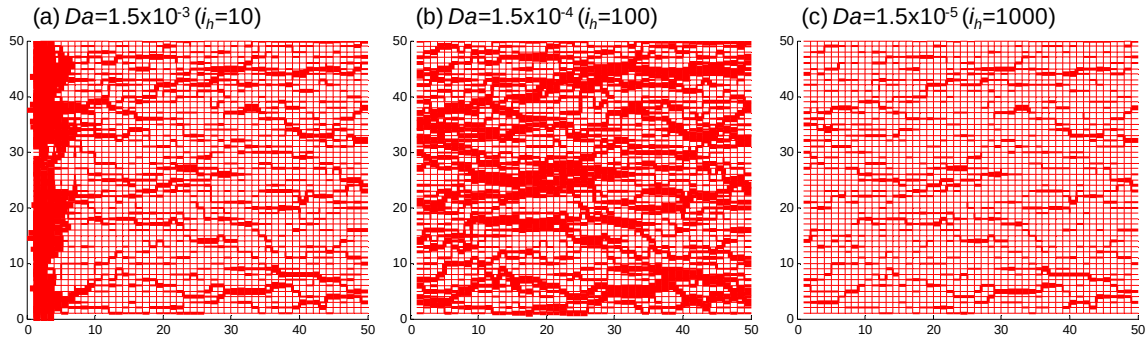

Mineral dissolution – Chemo-mechanical effects

Dissolution is performed in a numerical 2D- and/or 3D-cell with zero-lateral strain side-walls (PFC-3D). Spherical particles with uniform grain size distribution are packed by randomly placing smaller grains in the cube and gradually expanding them under zero gravity and zero interparticle friction to attain the target porosity. Then, friction and gravity are turned on, and the specimen is incrementally loaded in the vertical direction under zero lateral strain conditions.

Dissolution under constant servo-controlled vertical stress and zero lateral strain $\varepsilon_h=0$ is simulated by gradually reducing the radius of selected particles. The ratio of the mean unbalanced force to the mean contact force is always smaller than 0.001 to ensure stable conditions throughout the dissolution processes.

Shear strain localization. Before dissolution, contact forces align preferentially in the vertical principal stress direction, and evenly distributed force chains are observed throughout; this situation changes severely during pressure solution. Figure below shows contact force chains and strain fields after pressure solution (Note: strain fields are computed as the gradient of accumulated displacements from the beginning of dissolution). Shear bands developed spontaneously, for both linear and quadratic dissolution rates, and in packings made of either free-rotating particles (HR=0%) or interlocked particles (hindered rotation HR=80%). When there is a free upper boundary, shear localization is more pronounced at depth and diffuses towards the free surface as pressure solution is

contact-force dependent. Shear bands form at steeper angles in packings with interlocked particles, in agreement with the higher global friction angle granular materials with interlocking. Shear bands are 12~15 particles thick. Marked force chains form inside shear bands at a characteristic angle of ~50-60° with the shear band (case dR/dt=α•FN & HR=0%). These strong force chains form and buckle as force-dependent dissolution progresses, and the evolution of dissolution is faster in bands than in wedges

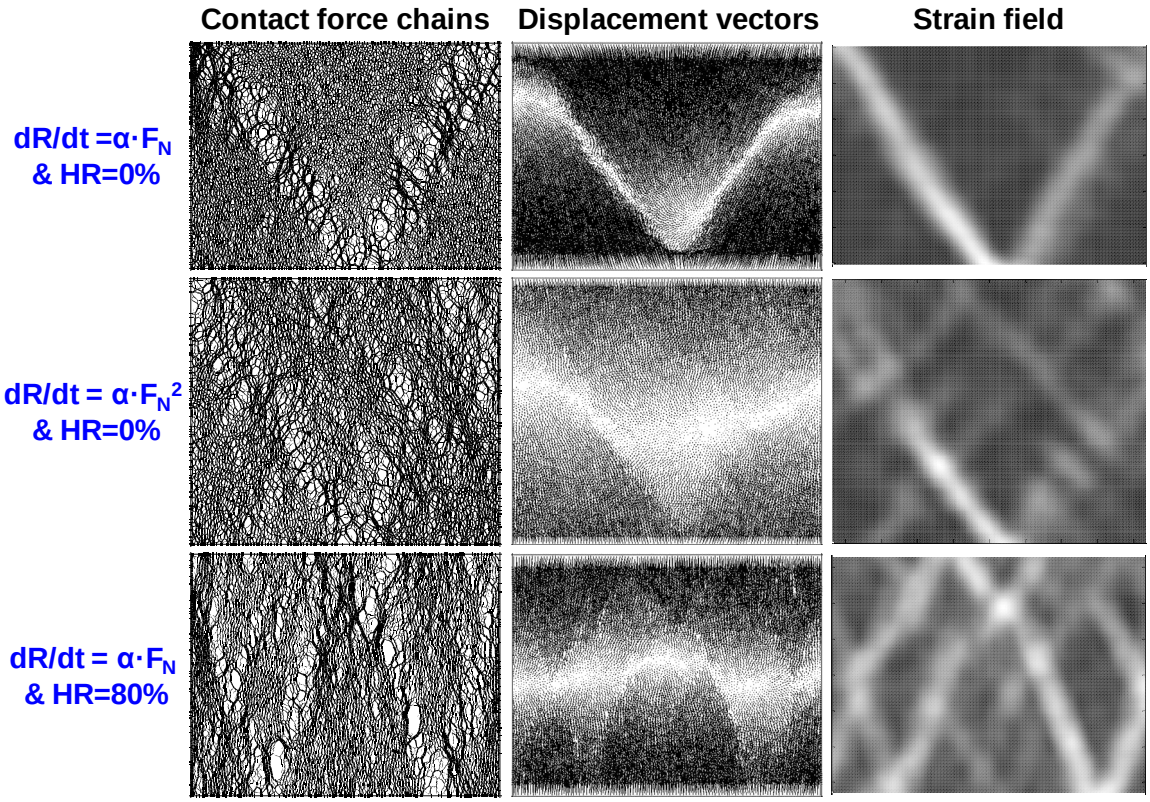

Caprock sealing efficiency - CO_2 Breakthrough and healing

We designed a high-pressure oedometer system to apply a constant vertical effective stress σ'_v<~3MPa, and withstand pore-fluid pressures P<~20MPa. Five oedometers are machined out of stainless steel 316 rods; effective stress is provided by a steel spring; and all seals are buna-N o-rings. Cells are designed to impose a radial fluid pressure gradient to cause flow from the periphery towards the drainage tube at the center of the specimen; this design seeks to minimize leaks between the specimen and chamber walls in standard 1D rigid-wall permeameters. The specimen is d_c~40mm in diameter and h~30mm to 35mm in height. We measure: (1) the input CO_2 pressure P_{in}[MPa] = P_{CO2} at the periphery at the reservoir side, (2) the exit pressure on the water side P_{out}[MPa] = P_w, (3) the amount

of water displaced during CO_2 invasion m_w [m^3], (4) the CO_2 flow rate after breakthrough q_{CO2} [m^3/s], and (5) the vertical deformation of the sediment specimen Δz[m] to cumpute the specimen volumetric strain $\varepsilon_v=\Delta z/h$. An auxiliary water-filled transparent pressure cell connected to the exit port is used to observe CO_2 leaks in the form of bubbles exiting the discharge pipe.

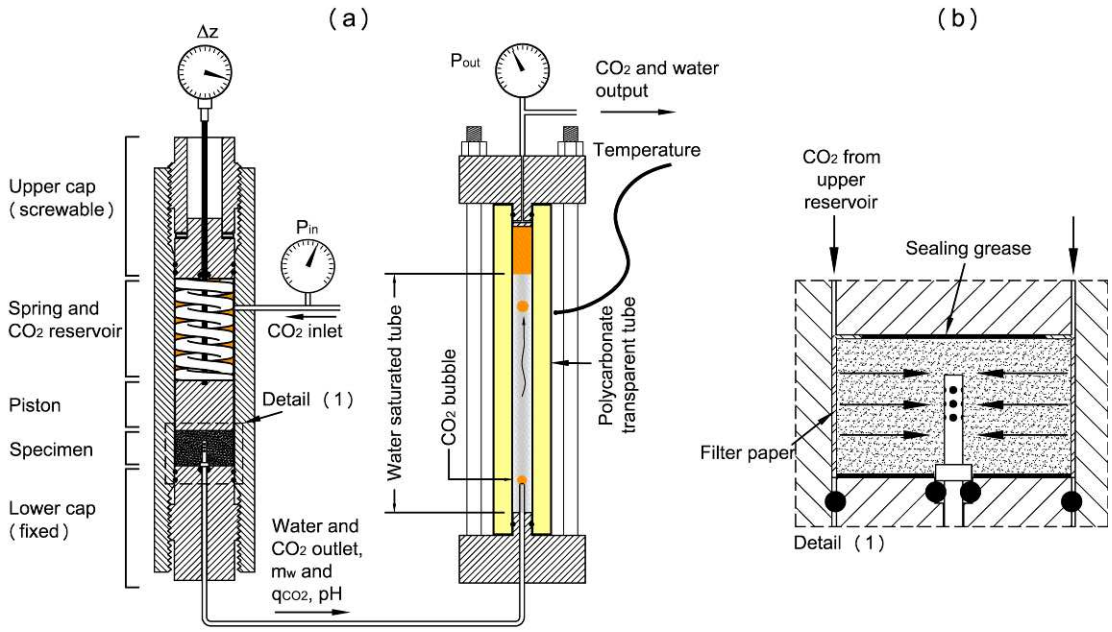

The water (or brine) and soil mixture is pre-compressed to an effective stress $\sigma`_v$~0.4MPa. Then, a cylindrical specimen is trimmed to fit the pressure cell. Filter paper is placed in between the oedometer walls and the specimen to create a homogeneous peripheral boundary flow condition. Sealing grease (non-reactive with CO_2 - Goop, Swagelok) is placed on the lower and upper pistons to prevent transport through these interfaces. Once in the cell, the specimen is consolidated to an effective stress $\sigma`_v$~2MPa. Then, we increase the peripheral CO_2 pressure P_{in}. In most experiments, the outlet water pressure is maintained at P_{out}=0.1MPa. The CO_2 inlet valve is closed after each pressurization cycle. A new pressure stage is initiated when settlement Δz, pressure P_{in}, and volume of displaced water mw approach asymptotic values. Eventually, CO_2 breaks through, and CO_2 flow rate q_{CO2} is monitored thereafter. Additional pressurization stages are used to measure the evolution of CO_2 permeability k_{CO2}.

Two sets of specimens were tested as part of this study. First, cores of the shale caprock from the southern Kansas CO_2 pilot test site were prepared for the required test geometry (outside diameter d_c~40mm, inside diameter d_p~3.17mm, height 25mm<h<35mm, polished upper and lower faces). Cores belong to Kinderhook-Chattanooga shale group (shale or shaly dolomudstones; porosity φ=0.04~0.08; permeability <0.01md).

Fines migration and accumulation at pore throats can clog and seal porous media. Herein, we attempt to seal cracks using suspensions of submicron-size particles in order to decrease the characteristic pore radius r_p within cracks. Suspensions are injected under a constant spring load equivalent to σ_v~1MPa, followed by further CO_2 injection. The selected water-based suspensions are prepared with bentonite (1gram of GEL-PureGold bentonite, and 20ml of water; S_s=400-800m^2/g) and kaolin (1gram SA1-Wilkinson kaolin, 1gram dispersant, and 20ml of water; S_s=10-20m^2/g).

The saturated shale-or-cement specimen was mounted into the high-pressure cell; epoxy was added at the lower interface and grease on the top interface to prevent boundary leaks between the specimen and the stainless steel caps. The spring applies a constant force equivalent to a vertical stress equal to σ_v~1MPa. Initially, water fills the annulus around the specimen. Two inlet pressure histories are imposed in this study (note: the outlet pressure is atmospheric in all cases). The first one involves a gradual increase in gas pressure until gas percolates throughout the specimen at the breakthrough pressure P_{bt} (Note: this method requires long testing times in intact rocks). Breakthrough is confirmed by continuous CO_2 leakage into the outlet pipette. The second test sequence starts with the injection of ~8ml of clay slurry under constant equivalent vertical stress σ_v~1MPa to flood the specimen (the volume of the annular gap between the test specimen and the high-pressure cell is 4ml). Then, we impose a CO_2 pressure significantly higher than the anticipated breakthrough pressure and close the inlet valve. The reservoir pressure decreases as water discharges until the residual shut-off pressure P_d is reached and CO_2 stops flowing. Specimens undergo a series of bentonite or kaolin slurry treatments and CO_2 re-injections.

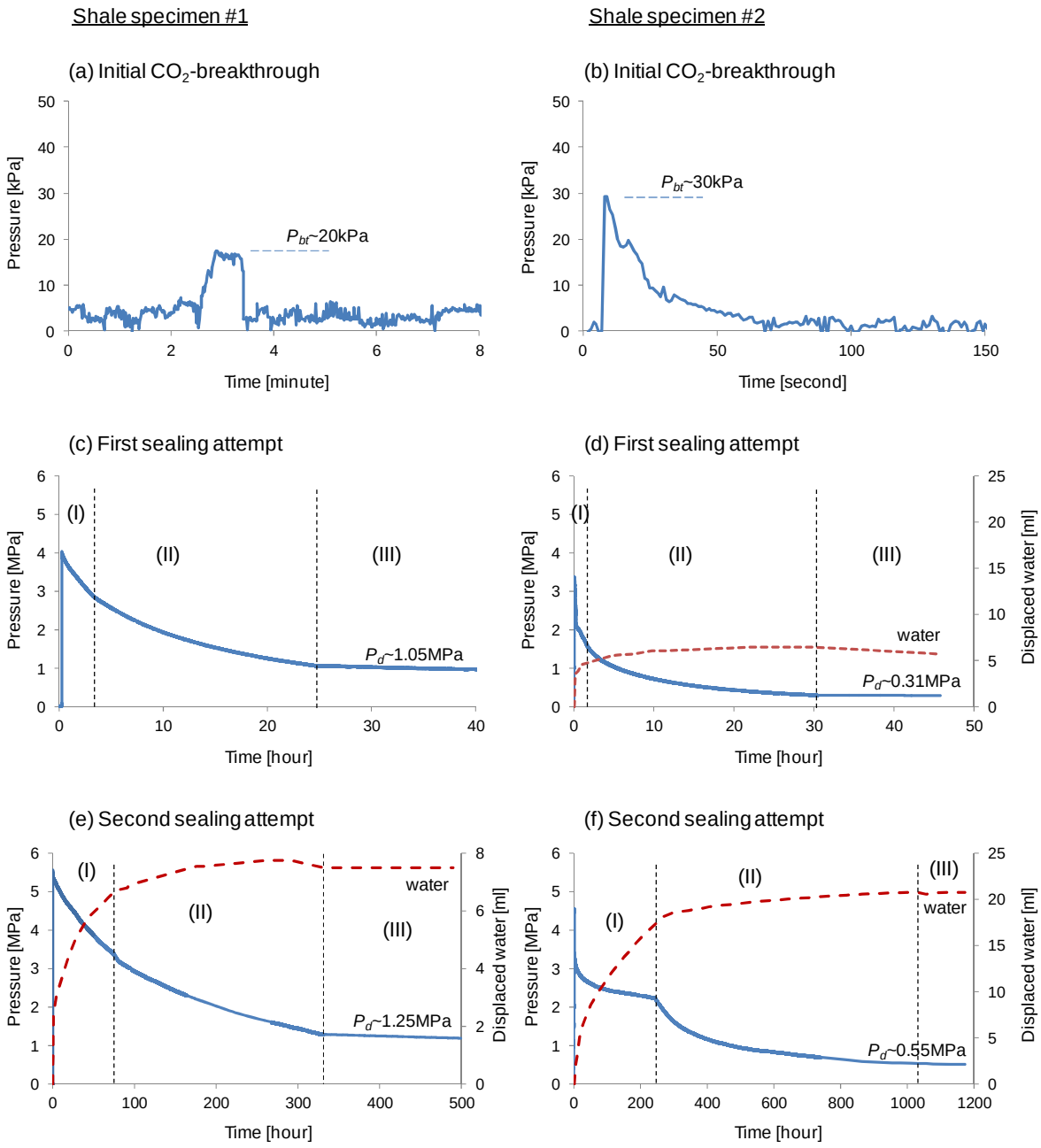

The three shale specimens exhibited very low CO_2-breakthrough pressures, ranging from P_{bt}≈10kPa-to-30kPa. This pressure range corresponds to 4μm~6μm pore radius (from $r_p=2T_s/P_{bt}$ where the interfacial tension is assumed as T_s=60mN/m under pressure P<1MPa), which is much larger than the nano-meter pore radius expected for these shales without cracks. For comparison, CO_2-brine entry pressures between 8kPa and 464kPa were estimated for the Chattanooga shale group based on mercury injection data. While visual inspection does not identify cracks, careful examination under the microscope reveals the presence of hairline cracks parallel to the bedding planes in all shale plugs. These cracks may have developed during coring and stress relaxation, and are parallel to the imposed flow direction in our test.

After the initial breakthrough tests, specimens underwent a series of bentonite or kaolin slurry treatments and CO_2 re-injections during sealing treatments. Results after sealing attempts show a marked increase in break-through pressure, and much lower water production and pressure decline rates after successive treatments. The water produced is transparent, without clays in suspension.

P-wave monitoring of hydrate-bearing sands during CH_4-CO_2 replacement

While previous studies have shown successful CH_4-CO_2 replacement in hydrates, the mechanical response of hydrate-bearing sediments during CO_2 injection, CH_4-CO_2 replacement, and CH_4 production needs to be adequately understood in order to avert production problems such as borehole instability, sand production, and buckling of the casing. We take advantage of the characteristics of elastic mechanical wave propagation in sediments to monitor CH_4 hydrate-bearing sands before, during, and after CO_2 injection. Results show that CH_4-CO_2 replacement occurs without a loss of stiffness in the granular medium. This implies that CO_2-flooded sandy reservoirs can remain mechanically stable during and after CH_4 gas production. On the other hand, pure CO_2 dissolves hydrate from the pore space, and continued sediment flushing with pure CO_2 reduces the degree of hydrate saturation, opens the pore throats, and weakens the granular skeleton. This phenomenon may cause a significant loss of strength near the injection points and regions subjected to high liquid CO_2 flow rate. The results of complimentary analyses show a decrease in bulk stiffness as water is displaced by liquid CO_2, a stiffening of the granular skeleton during hydrate formation at contacts (diffusion limited), and the implications of water solubility in liquid CO_2.

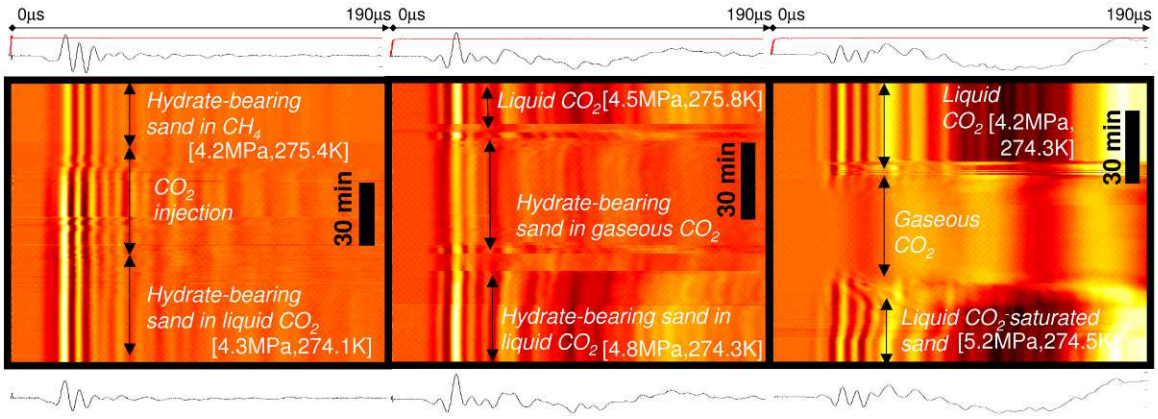

CONCLUSIONS

The goals of this project were to addresses emergent hydro-chemo-mechanically coupled phenomena, their implications on CO_2 geological storage, self-healing, and engineered CO_2 injection method. The scope of work included general analyses of parameter domain, interfacial properties of water, mineral, CO_2 and/or surfactant system, interaction between clay particles and CO_2, reactive fluid flow as a result of CO2 dissolution, two-phase flow between immiscible CO2 and formation fluid, CO_2 breakthrough and CO_2 permeability, sealing strategies, and CH_4-CO_2 hydrate replacement and hydro-mechanical implications. Complementary analyses, numerical simulations, and experimental studies were used to advance the work. The main observations are grouped in categories as follows.

General hydro-chemo-mechanical analyses and implications.

- In horizontal zero-dip stratigraphies (i.e., no geometric trap), the CO_2 pool thickness will be limited by lateral capillary trapping rather than by the reservoir layer thickness. Typical pools will be only a few meters thick in the absence of geometric traps.
- Brine densifies as CO_2 and minerals in the reservoir dissolve. Density changes are more pronounced when the brine salinity is low; the maximum increase in brine density is ~1.2%. The ensuing convection may have a characteristic time scale as short as a few years in permeable reservoirs. The maximum decrease in mineral volume at equilibrium is less than 0.2% for a closed system (Dissolution). The associated increase in permeability can be as high as 3% for each pore volume of brine that completely reacts with the host medium (Precipitation). Dissolution localization and convective currents with short time scale can significantly magnify dissolution effects and lead to pronounced long-term consequences.
- Convection-sustained mineral dissolution causes a decrease in horizontal effective stress and the sediment may reach the Rankine active failure condition. Either compaction-driven shear failure of the reservoir or caprock bending failure above dissolving reservoir zones may occur as a result of mineral dissolution. In particular, the unsupported free span of the caprock cannot exceed 20% of the caprock thickness for typical reservoir conditions.
- The continuous influx of dry CO_2 dries residual brine near the wellbore. The precipitation of secondary minerals increases the mineral volume by a maximum of 5% in the patches with residual brine saturation. The anticipated decrease in CO_2 permeability is less than 20%.

Water-CO_2-mineral systems: Interfacial tension, contact angle and diffusion.

- CO_2-water interfacial tension decreases significantly from 72mN/m to ~25mN/m as pressure increases to reservoir pressure-temperature conditions.
- Contact angle varies with CO_2 pressure in response to changes in CO_2-water interfacial tension.

- Water solubility and diffusivity in liquid CO_2 govern the evolution of interparticle pendular water.
- Pressure-dependent interfacial tension and contact angle affect injection patterns and breakthrough mechanisms.

Engineered CO_2 injection.

- Surfactants that have hydrophilic heads and CO_2-philic tails lower the interfacial tension between CO_2 and water. The long-chain nonionic surfactant used in these experiments (weight percent≈0.4%) lowered the CO_2-water interfacial tension from 50mN/m to ~4mN/m at pressure $P \geq 7$MPa.
- The contact angle formed by a water-surfactant droplet resting on a glass substrate and surrounded by CO_2 increases from $\theta \sim 20°$ at P=0.1MPa to $\theta \sim 70°$ at P=10MPa. Reduced interfacial tension γ_{fl} and larger contact angle θ combine to produce a marked decrease in the capillary factor $\gamma_{fl} \bullet cos\theta$.
- Experimental CO_2 injection tests in pore micro-models and parallel network model simulations demonstrate that the sweep efficiency of CO_2 invasion can be effectively enhanced by lowering the capillary factor $\gamma_{fl} \bullet cos\theta$. In particular, the sweep efficiency can double with the addition of surfactants.
- Engineered CO_2 injection such as using surfactants can optimize pore space occupancy underground and minimize emergent hydro-chemo-mechanically coupled phenomena such as salt precipitation near the well (lower injection difficulties), water acidification and mineral dissolution (lower possibility of piping, internal shear, and differential settlement), and long-term convective flow. Consequently, improved long-term integrity of storage reservoirs is anticipated.

Clay interaction with liquid and supercritical CO_2.

- The electrical interaction between clay particles changes when CO_2 displaces water from the pore space. The analysis of inter-particle forces shows a decrease in electrical repulsion and an increase in attraction. In particular, Lifschitz theory predicts a three-fold increase in the Hamaker constant from clay-water-clay to clay-CO_2-clay systems.
- The change in electrical forces and the emergence of capillary effects anticipates volume contraction following the injection of CO_2 in initially water-saturated formations.
- Open-mode fractures could develop in normally consolidated clayey seals even when the burial depth exceeds 1 km. Localized CO_2 flow would ensue and hinder the sealing capacity of caprocks.
- Complex interplay between chemo-hydro-mechanical processes may lead to positive feedback mechanisms that can either degrade (e.g., platelet collapse → increase in pore size → further fluid conduction) or self-stabilize (e.g., water

dissolution in CO_2 → salt precipitation from brine → porosity reduction) the caprock seal capacity, or alter CO_2 injectivity into the reservoir.

Reactive fluid transport as a consequence of CO_2 injection.

- The concentration of reactant species rapidly decreases near the inlet of a porous network when the hydraulic gradient i_h is low and Damköhler number exceeds $Da>10^{-4}$. Reactant species migrate towards the outlet of a porous network and ramify as the hydraulic gradient increases and the Damköhler number drops $Da<10^{-4}$.
- At low hydraulic gradients ($Da>10^{-4}$; $i_h<100$), tube diameter enlargement prevails near the inlet, flow remains more homogeneous, and high inlet pressure is gradually transferred further into the formation. As hydraulic gradients increase ($Da<10^{-4}$; $i_h>100$), pore enlargement extends towards the outlet and reactive flow tends to preferentially enlarges tubes with high flow rate.
- Both the Damköhler number and pore-size variability affect the relationship between mean tube diameter and flow rate. Changes in Damköhler number result in inherent bias between average and local trends. The exponent of the Kozeny-Carman-type equation $q/q_0=(\varphi/\varphi_0)^{\alpha}$ increases with the coefficient of variation COV in pore size. Both the Damköhler number and pore-size variability should be accounted in field-scale FEM models.

Dissolution - Pressure solution and shear band localization

- Dissolution causes global contraction. Pressure solution promotes densification during early stages of dissolution, even in the absence of reprecipitation. High friction/interlocking hinders global contraction but leads to a higher increase in porosity.
- Horizontal stress may drop to k_a in high friction/interlocking sediments. Shear localization naturally emerges in pressure solution.
- Hydro-chemical coupling can lead to dissolution localization (pipes or wormholes) as the result of the positive feedback that involves changes in porosity and reactive transport. Marked force chains are preferentially vertical away from pipes, yet, they are preferentially horizontal within pipes. Horizontal contact forces inside pipes prevent the buckling of granular columns in the stable zones.

Caprock sealing efficiency and integrity

- Breakthrough pressure, ensuing CO_2 permeability, and specimen volumetric deformation were measured on sediment plugs using specially designed high pressure oedometers. Results show that the breakthrough pressure increases as the pore size decreases (1:1 slope in log-log space), and it is 1MPa<P^*<3MPa for kaolinite and bentonite plugs consolidated to $\sigma`_v$~2MPa.

- Bentonite plugs developed fluid-driven open-mode fractures that limited their capillary breakthrough pressure. The post breakthrough CO_2 permeability was higher than anticipated for these fine grained sediments.
- The sediment dries during CO_2 transport. Electrical resistivity and magnetic resonance data show higher drying close to the drainage pipe (radial flow). CO_2 permeability after breakthrough increases by orders of magnitude with continued CO_2 advection. Most specimens showed a final water saturation of 0.7-0.9.
- Order of magnitude analyses show that leaks in most storage sites will be advection-controlled once percolation takes place (in the absence of high conductivity geological features). Diffusive and advective CO_2 leaks through non-fractured caprocks will be minor and will not compromise the storage capacity of CO_2 injection sites.

CO_2 Breakthrough for shale and conditions for self-healing

- While pores in shales and cements are in the nm-scale and can sustain MPa-scale capillary pressures, orders of magnitude lower breakthrough pressures are measured when specimens contain micron-thick discontinuities.
- Suspensions of sub-micron clay particles can be injected to fill cracks. Sealing treatments cause a marked increase in the shut-off pressure, and a pronounced decrease in leak rates can be attained as the specimen is subjected to successive sealing treatments. In particular, shales with hairline cracks can experience an increase in breakthrough pressure from ~30kPa before treatment to more than P~1MPa after sealing treatments with clay slurries.
- Intact cement plugs can sustain a shut-off pressure in excess of P_d~6MPa. Extensive carbonation and reaction rims around grains are readily observed in short-duration tests where water saturated cement plugs are exposed to supercritical CO_2. Reactions should be slower once CO_2 dries the cement.
- The design of suspensions for field applications must take crack aperture and reservoir permeation into consideration. The use of dispersants or buoyant particles would extend the reach of suspension-based sealing.

P-wave monitoring of hydrate-bearing sand during CH_4-CO_2 replacement.

- CH_4-CO_2 replacement within the stability field occurs without loss of stiffness in the granular medium.
- CO_2-flooded sandy reservoirs can remain mechanically stable during and after CH_4 gas production.
- Continued sediment flushing with dry CO_2 dissolves the hydrate, opens the pore throats, and weakens the granular skeleton.

TRAINING OF HIGHLY QUALIFIED PERSONNEL

- Dr. Nicolas Espinoza (2011). CO2 sequestration – Fundamental Studies. Current Position: Assistant Professor, University of Texas at Austin.
- Dr. Seunghee Kim (2012). CO2 sequestration – Hydro-chemo-mechanical analyses. Current Position: Postdoctoral Fellow, Bureau of Economic Geology, Austin.

Also (partial involvement)

- Minsu Cha (2012). Mineral Dissolution - Implications. Current Position: Research Fellow, Colorado School of Mines.
- Jong Won Jung (2010). Gas Production from Methane Hydrates. Current Position: Assistant Professor, Louisiana State University.
- Hosung Shin (2009). Discontinuities. Current Position: Assistant Professor, Ulsan University.
- Sylvain Cardon (2010), CO2 Storage: Dissolution and Ko, from Université Joseph Fourier, Grenoble, France.
- Stefanos Athanasopoulos (2013), Grouting and leakage, from Université Joseph Fourier, Grenoble, France.

PUBLICATIONS

Refereed Journals

Submitted

Kim, S. H. and Santamarina, J. C. (2013). Reactive Fluid Flow in CO2 Storage Reservoirs – Pore Network Model Study (submitted 11/2013)

Kim, S. H. and Santamarina, J. C. (2013). Reactive Fluid Flow in CO2 Storage - Rock Fracture (submitted 11/2013).

Cha, MS and Santamarina, J.C., Localized dissolution, Journal Geophysical Research (submitted 7/16/2013).

Cha, MS and Santamarina, J.C., Pressure-dependent Mineral Dissolution – Shear Discontinuities, Geology (submitted 10/10/2013) .

Cha, MS and Santamarina, J.C., Dissolution of Randomly Distributed Soluble Grains: Post Dissolution k0-Loading and Shear, Geotechnique, (submitted 7/10/2013) .

Kim, S. H. and Santamarina, J. C. (2013). CO_2 Geological Storage: Hydro-Chemo-Mechanical Analyses and Implications, Greenhouse Gases: Science and Technology (submitted 8/19/2013).

In Print

Kim, S. H. and Santamarina, J. C. (2013). Engineered CO2 injection for geological storage - The Use of Surfactants, International Journal of Greenhouse Gas Control.

Published

Kim, S. H. and Santamarina, J. C. (2013). CO_2 breakthrough and leak-sealing – Experiments on shale and cement, International Journal of Greenhouse Gas Control, vol. 19, pp.

Espinoza, D.N. and Santamarina J.C., (2012), Clay interaction with liquid and supercritical CO2: The relevance of electrical and capillary forces, International Journal of Greenhouse Gas Control, vol. 10, pp. 351-362.

Shin H. and Santamarina J.C. (2011), Desiccation Cracks in Saturated Fine-Grained Soils: Particle Level Phenomena and Effective Stress Analysis, Geotechnique, vol. 61, pp. 961–972.

Espinoza, D.N. and Santamarina, J.C. (2011), P-wave monitoring of hydrate-bearing sand during CH4-CO2 replacement, Int. J. Greenhouse Gas Control, doi: 10.1016/j.ijggc.2011.02.006.

Santamarina, J.C. and Cho, G.C. (2011), Energy Geotechonology, KSCE Journal of Civil Engineering, vol. 15, no. 4, pp. 607-610.

Espinoza, D.N., Kim, S.H., Santamarina, J.C. (2011), Carbon Geological Storage, KSCE Journal of Civil Engineering, vol. 15, no. 4, pp. 707-719.

Jung, J.W., Espinoza, D.N. and Santamarina, J.C. (2010), Hydrate Bearing Sediments: CH_4-CO_2 Replacement, Journal of Geophysical Research, vol. 115, B10102, doi:10.1029/2009JB000812

Jung, J.W. and Santamarina, J.C. (2010), CH_4-CO_2 Replacement in Hydrate-Bearing Sediments: A Pore-Scale Study, G-Cubed Geochemistry, Geophysics and Geosystems, Vol. 11, Q0AA13, doi:10.1029/2010GC003339.

Espinoza, D.N. and Santamarina J.C. (2010), Water-CO2-mineral systems: interfacial tension, contact angle and diffusion – Implications to CO2 geological storage, Water Resources Research, vol. 46, DOI: 10.1029/2009WR008634.

Shin, H., Santamarina, J.C. and Cartwright, J. (2010), Displacement Field In Contraction Driven Faults, J. Geophysical Research, 115, B07408, doi:10.1029/2009JB006572.

Special Contributions and Review Articles (Non-Refereed Journals)

Santamarina, J.C. and Jang, J. (2010), Energy Geotechnology: Implications Of Mixed Fluid Conditions, Proc. 5th International Conference on Unsaturated Soils, Unsat 2010, Barcelona, Eds. A. Gens and E. Alonso.

Publications in Conference Proceedings - Others

Kim, S. and Santamarina, J.C. (2014), Geological CO2 Storage: Reactive Fluid Transport - Pore-Scale Study, ASCE GeoCongress, Atlanta.

Bang, ES, Son, JS and Santamarina, J.C., Subsurface CO_2 Leakage: Lab-Scale Study of Salient Characteristics and Assessment of Borehole-Based Detection Using Resistivity Tomography. 4th International Conference on Geotechnical and Geophysical Site Characterization (ISC'4), Porto de Galinhas, Pernambuco – Brazil, September 2012.

Santamarina, J.C. (2012), Energy Geotechnology, *Geo-Strata*, pp. 14-15.